UNIT CIRCLE MVDR BEAMFORMER

Saurav R. Tuladhar, John R. Buck *

University of Massachusetts Dartmouth
Electrical and Computer Engineering Department
North Dartmouth, Massachusetts, USA

ABSTRACT

The array polynomial is the z-transform of the array weights for a narrowband planewave beamformer using a uniform linear array (ULA). Evaluating the array polynomial on the unit circle in the complex plane yields the beampattern. The locations of the polynomial zeros on the unit circle indicate the nulls of the beampattern. For planewave signals measured with a ULA, the locations of the ensemble MVDR polynomial zeros are constrained on the unit circle. However, sample matrix inversion (SMI) MVDR polynomial zeros generally do not fall on the unit circle. The proposed unit circle MVDR (UC MVDR) projects the zeros of the SMI MVDR polynomial radially on the unit circle. This satisfies the constraint on the zeros of ensemble MVDR polynomial. Numerical simulations show that the UC MVDR beamformer suppresses interferers better than the SMI MVDR and the diagonal loaded MVDR beamformer and also improves the white noise gain (WNG).

Index Terms— adaptive beamformer, MVDR, array polynomial

1. INTRODUCTION

Beamformers enhance signals arriving at an array from a desired look direction while suppressing interferers and noise. Conventional beamformers (CBFs) using a delay-and-sum approach have limited ability to suppress loud interferers which can leak through the high sidelobes of the CBF beampattern and mask weaker signal of interest. Adaptive beamformers (ABF) place notches in the direction of interferers to suppress the interferer power at the output and improve signal-to-interferer-plus-noise ratio (SINR) [1]. The minimum variance distortionless response (MVDR) beamformer is one of the most commonly used ABFs [2]. In practice, the ensemble covariance matrix (ECM) is unknown so the sample covariance matrix (SCM) replaces the ECM to compute the ABF weights. The resulting ABF is known as the Sample Matrix Inversion (SMI) MVDR beamformer [1].

The beampattern defines the spatial response of a beamformer [1]. The beampattern of a beamformer using a ULA can be represented as an array polynomial by taking z-transform of beamformer weights [3]. This is analogous to the system function representation of a discrete time (DT) LTI filter by taking z-transform of its impulse response [4]. As with DT LTI filters, beamformers also have a pole-zero representation in the complex plane and continuing the analogy, the beampattern is obtained by evaluating the array polynomial on the unit circle. The array polynomial zeros generally correspond to the beampattern notches but when the zeros fall on the unit circle they result in perfect notches or nulls.

*Supported by ONR grant N00014-12-1-0047.

The zeros of an ensemble MVDR beamformer polynomial for narrowband planewave are constrained on the unit circle. However, the SMI MVDR array polynomial zeros generally do not lie on the unit circle. A new beamformer is developed by radially projecting the SMI MVDR zeros on the unit circle and satisfying the constraint on the ensemble MVDR zeros. The proposed unit circle MVDR (UC MVDR) beamformer suppresses interferers better than the SMI MVDR and the diagonal loaded MVDR beamformer and at the same time improves white noise gain (WNG) performance.

Prior work involving the use of array polynomial representation for beamforming includes work by Steinberg [5]. Steinberg discusses the polynomial representation of radiation pattern of uniform antenna arrays and presents an approach to synthesize radiation patterns by manipulating zero locations on the unit circle. The methods presented in [5] are limited to ensemble cases. Several proposed adaptive notch filters for DT signals constrain the filter poles and zeros to render 'sharper' notches in their frequency response [6–8]. However these approaches are based on DT IIR filters while beamformers with ULAs are analogous to DT FIR filters.

The remainder of this paper is organized as follows: Sec. 2 reviews the signal model, MVDR beamformer and the metrics used to evaluate beamformer performance. Sec. 3 develops the polynomial representation for ULA beamformers and discusses zero locations for the MVDR and SMI MVDR beamformers. Sec. 4 presents the UC MVDR beamformer algorithm. Sec. 5 discusses the simulation results comparing the performance of the UC MVDR with SMI MVDR and DL MVDR.

2. BACKGROUND

The narrowband planewave data measured on an N element ULA is modeled as an $N \times 1$ complex vector,

$$\mathbf{x} = \sum_{i=1}^{D} a_i \mathbf{v}_i + \mathbf{n} \tag{1}$$

where D is the number of planewave signals, a_i is i^{th} signal amplitude and $\mathbf{n}$ is the noise sample vector. The amplitude is modeled as a zero mean complex circular Gaussian random variable, i.e., $a_i \sim \mathcal{CN}(0, \sigma_i^2)$ and the noise is assumed to be spatially white with complex circular Gaussian distribution, i.e., $\mathbf{n} \sim \mathcal{CN}(\mathbf{0}, \sigma_w^2 \mathbf{I})$. The complex vector $\mathbf{v}_i$ is the narrowband planewave array manifold vector defined as,

$$\mathbf{v}_i = [1,\ e^{-j(2\pi/\lambda)du_i},\ e^{-j(2\pi/\lambda)2du_i}, \ldots, e^{-j(2\pi/\lambda)(N-1)du_i}]^{\mathrm{T}},$$

where $u_i = \cos(\theta_i)$ and θ_i is the i^{th} signal direction, λ is the wavelength, d is the ULA inter element spacing and $[\cdot]^T$ denotes transpose. In the sequel, signal direction will be represented in terms of

u. Assuming the D signals to be uncorrelated in (1), the ECM is,

$$\mathbf{\Sigma} = E[\mathbf{x}\mathbf{x}^{\mathrm{H}}] = \sum_{i=1}^{D} \sigma_i^2 \mathbf{v}_i \mathbf{v}_i^{\mathrm{H}} + \sigma_w^2 \mathbf{I}. \quad (2)$$

where σ_i^2 is i^{th} signal power and σ_w^2 is the noise power at each sensor.

The narrowband planewave MVDR beamformer weight vector for a ULA is,

$$\mathbf{w}_{\mathrm{MVDR}} = \frac{\mathbf{\Sigma}^{-1}\mathbf{v}_0}{\mathbf{v}_0^{\mathrm{H}}\mathbf{\Sigma}^{-1}\mathbf{v}_0}, \quad (3)$$

where $\mathbf{v}_0$ is the array manifold vector for the look direction $u_0 = \cos(\theta_0)$. Computing the MVDR weights in (3) requires knowledge of the ECM but in practical applications the ECM is unknown *a priori*. Consequently, the MVDR ABF is approximated by the SMI MVDR computed by replacing the ECM $\mathbf{\Sigma}$ in (3) with the SCM,

$$\mathbf{S} = \frac{1}{L}\sum_{l=1}^{L} \mathbf{x}_l \mathbf{x}_l^{\mathrm{H}}$$

where the L is the number of data snapshots and $\mathbf{x}_l$ is the data snapshot vector in (1). In practice, the number of data snapshots available to compute the SCM are limited either due to physical or stationarity constraints of the environment [9][10]. When the number of snapshots is on the order of the number of array elements, i.e., $N \approx L$, the SCM is ill-conditioned for inversion. The resulting SMI MVDR beamformer suffers from a distorted beampattern with high sidelobes and subsequent loss in SINR [11][12]. In this scenario, a common approach is to apply diagonal loading (DL) to the SCM to get $\mathbf{S}_\delta = \mathbf{S} + \delta\mathbf{I}$ where δ is the DL factor. This results in the DL MVDR beamformer. DL makes SCM inversion stable, provides better sidelobe control and improves beamformer WNG [13]. An appropriate choice for the DL factor requires knowledge of the signal and the interference plus noise power levels which are unknown in practice. Some of the proposed methods to choose DL factor are either ad-hoc in nature or require numerical solutions to optimization problems [13].

The beampattern defines the complex gain due to the beamformer on a unit amplitude planewave from direction $u = \cos(\theta)$, i.e.,

$$\mathrm{B}(u) = \mathbf{w}^H \mathbf{v}(u) = \sum_{n=0}^{N-1} w_n^* \left(e^{-j\frac{2\pi}{\lambda}du}\right)^n \quad (4)$$

where $(\cdot)^*$ denotes conjugate and $-1 \leq u \leq 1$ is the direction range of the beampattern. In the presence of strong interfering signals, a beamformer's ability to suppress the interferers is quantified by the notch depth (ND) defined as $\mathrm{ND} = |\mathrm{B}(u_1)|^2$, where u_1 is the interferer direction. ABFs aim to improve SINR by adjusting the ND and location based on interferer power and direction.

White noise gain (WNG) is defined as the array gain when the noise is spatially white. Assuming unity gain in the look direction, $\mathrm{WNG} = ||\mathbf{w}||^{-2}$ where $||\cdot||$ denotes the Euclidean norm [1]. WNG is also a metric for beamformer robustness against mismatch [14]. The CBF has the optimal WNG which is equal to the number of array sensors N [15].

3. BEAMFORMER POLYNOMIAL

The beampattern of a narrowband planewave beamformer with ULA can be represented as a complex polynomial [3][5]. For a standard ULA with $d = \lambda/2$,

$$\mathrm{B}(u) = \sum_{n=0}^{N-1} w_n^* (e^{-j\pi u})^n. \quad (5)$$

Letting $z = e^{j\pi u}$ in (5), we get the array polynomial

$$\mathrm{P}(z) = \sum_{n=0}^{N-1} w_n^* z^{-n} = \mathcal{Z}(\mathbf{w}^{\mathrm{H}}). \quad (6)$$

$\mathrm{P}(z)$ is an $N-1$ degree polynomial in the complex variable z with beamformer weights (w_n^*) as its coefficients. Eq. (6) is in the form of the z-transform of the conjugate beamformer weights [4, Chap.3]. This polynomial representation maps the bearing variable u into the complex plane. The phase of the complex variable is related to the bearing variable as $\arg(z) = \omega = \pi u$. Evaluating (6) on the unit circle $\{z \in \mathbb{C}, |z| = 1\}$ returns it to (5). Hence the zeros of $\mathrm{P}(z)$ on the unit circle correspond to nulls of the beampattern.

The MVDR polynomial is obtained as

$$P_M(z) = \mathcal{Z}(\mathbf{w}_{\mathrm{MVDR}}^{\mathrm{H}}) = \Gamma \prod_{n=1}^{N-1} (1 - \zeta_n z^{-1}), \quad (7)$$

where Γ is a scaling term and ζ_n are the ensemble MVDR zeros. Figure 1 shows MVDR zeros for an example case of $N = 11$ element ULA and a single interferer at $u_1 = 3/N$. All MVDR zeros in Figure 1 are on the unit circle. In fact the MVDR ensemble zeros are always constrained on the unit circle for planewave beamforming using a ULA. The unit circle constraint was initially discovered and proved by Seinhardt and Guerci but the result does not appear to be widely known [16].

However, the SMI MVDR zeros are perturbed from the ensemble MVDR zero locations and are randomly located on the complex plane about the ensemble MVDR zero locations. The SMI MVDR zeros do not necessarily lie on the unit circle and they correspond to notches in the SMI MVDR beampattern. Any zeros that fall closer to the origin or far outside the unit circle have negligible contribution to beampattern [4, Chap. 5]. The following section describes how the SMI MVDR beamformer can be modified by moving the sample zeros to the unit circle following the constraint on ensemble zeros.

4. UNIT CIRCLE MVDR BEAMFORMER

The unit circle MVDR (UC MVDR) beamformer projects the SMI MVDR zeros radially on the unit circle consistent with the constraint on the ensemble MVDR zeros. By placing zeros on the unit circle, the UC MVDR beampattern guarantees nulls in the direction corresponding to the zeros. Figure 2 describes the UC MVDR beamformer algorithm. The algorithm begins from the SMI MVDR weights $\mathbf{w}_{\mathrm{SMI}}$ computed using the SCM. The z-transform of the elements of $\mathbf{w}_{\mathrm{SMI}}^{\mathrm{H}}$ gives the SMI MVDR polynomial

$$P_S(z) = G \prod_{n=1}^{N-1} (1 - \xi_n z^{-1}),$$

where G is a scaling factor, $\xi_n = r_n e^{j\omega_n}$ are the SMI MVDR zeros and the r_ns are generally not unity. Each SMI MVDR zero ξ_n is moved radially to the unit circle to obtain the UC MVDR zeros $\hat{\xi}_n = e^{j\omega_n}$. An exception is made when the SMI MVDR zeros fall within the CBF main-lobe region in the complex plane. Such zeros are moved to the CBF first-null location on the unit circle to protect the

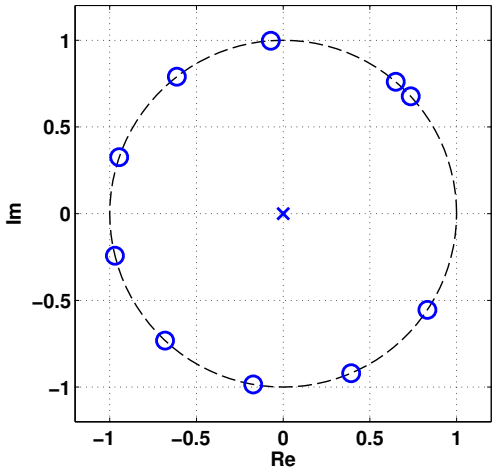

Fig. 1. Zero locations of MVDR beamformer using $N = 11$ element ULA.

main-lobe. A unit circle polynomial $P_{UC}(z)$ is defined using the new unit circle zeros $\hat{\xi}_n$s,

$$P_{UC}(z) = \prod_{n=1}^{N-1}(1 - \hat{\xi}_n z^{-1}) = \sum_{n=0}^{N-1} c_n^* z^{-1}. \quad (8)$$

The coefficients c_ns are the new beamformer weights. The resulting beamformer will have beampattern nulls in the direction corresponding to $\hat{\xi}_n$. Finally, the c_ns are scaled to ensure the beamformer has unity gain in the look direction to satisfy the distortionless constraint of a MVDR beamformer. The resulting UC MVDR beamformer weight vector is $\mathbf{w}_{\rm UC} = \mathbf{c}/|\mathbf{c}^{\rm H}\mathbf{v_0}|$ where $\mathbf{c} = [c_0, c_2 \ldots c_{N-1}]$ and $\mathbf{v}_0$ is the array manifold vector for look direction $u_0 = \cos(\theta_0)$. Since polynomial zero locations are invariant to coefficient scaling, the UC MVDR beampattern will still have nulls in the same locations as $P_{UC}(z)$.

Figure 3 shows a representative example of zero locations and beampattern of a UC MVDR compared with SMI MVDR beamformer using $N = 11$ element ULA and $L = 12$ snapshots. A single interferer is present at $u_1 = \cos(\theta) = 3/N$. In Figure 3a, the green diamond markers indicate the SMI MVDR zero locations and the red circle markers indicate the UC MVDR zeros obtained by moving the SMI MVDR zeros to unit circle. The corresponding beampattern plots in Figure 3b show perfect notches and lower sidelobes in the UC MVDR beampattern (solid red) in contrast to shallow notches and higher sidelobes in the SMI MVDR beampattern (dot-dash green).

5. SIMULATION RESULTS

Figure 4 compares the empirical CDF of output power in the interferer direction for the UC MVDR beamformer against the SMI MVDR and DL MVDR beamformers. The CDF curves are based on 5000 Monte Carlo trials. The dashed vertical line represents the ideal output power using the ensemble MVDR beamformer. The ULA size was $N = 11$ and a single interferer was fixed at $u_1 = \cos(\theta_1) = 3/N$ for each trial. The sensor level INR was 40 dB. The SCM was computed using $L = 12$ snapshots. The DL level was set to keep the mean WNG for UC MVDR and DL MVDR beam-

1: Compute SCM : $\mathbf{S} = \frac{1}{L}\sum_{n=1}^{N} \mathbf{x}\mathbf{x}^{\rm H}$
2: Compute SMI MVDR weights : $\mathbf{w}_{\rm SMI} = \mathbf{S}^{-1}\mathbf{v}_0/(\mathbf{v}_0\mathbf{S}^{-1}\mathbf{v}_0)$
3: $P_S(z) = \mathcal{Z}(\mathbf{w}_{\rm SMI}^{\rm H}) = G\prod_{n=1}^{N-1}(1 - \xi_n z^{-1})$ and $\xi_n = r_n e^{j\omega_n}$
4: **if** $|\omega_n| > 2\pi/N$ **then**
5: $\quad \hat{\xi}_n = e^{j\omega_n}$
6: **else if** $|\omega_n| \leq 2\pi/N$ **then**
7: $\quad \hat{\xi}_n = e^{j{\rm sgn}(\omega_n)2\pi/N}$
8: **end if**
9: Use $\hat{\xi}_n$ to create new unit circle polynomial :
$\quad P_{UC}(z) = \prod_{n=1}^{N-1}(1 - \hat{\xi}_n z^{-1}) = \sum_{n=0}^{N-1} c_n^* z^{-n}$
10: Define : $\mathbf{c} = [c_1, c_2 \ldots c_N]$
11: UC MVDR weight : $\mathbf{w}_{\rm UC} = \mathbf{c}/|\mathbf{c}^{\rm H}\mathbf{v}_0|$

Fig. 2. UC MVDR beamformer algorithm

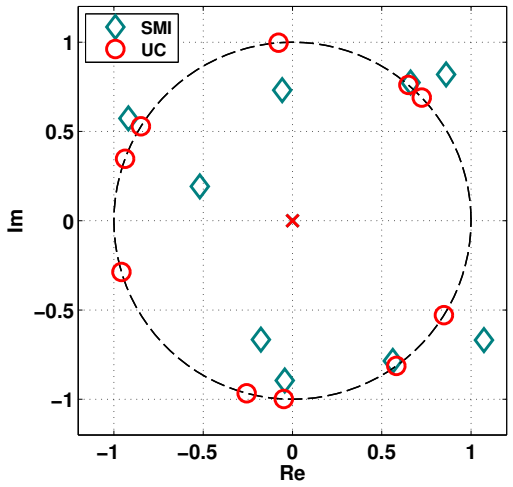

(a)

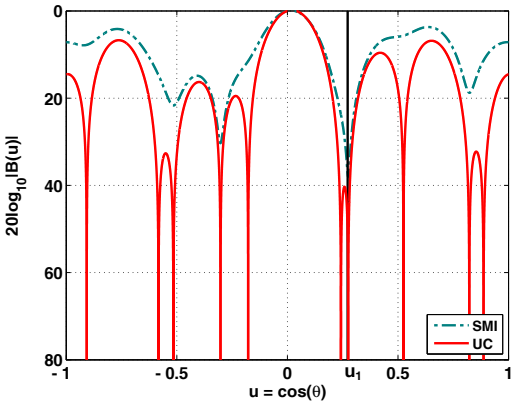

(b)

Fig. 3. Zero locations and beampattern for representative example of SMI MVDR and UC MVDR beamformer using $N = 11$ element ULA for $L = 11$ snapshots.

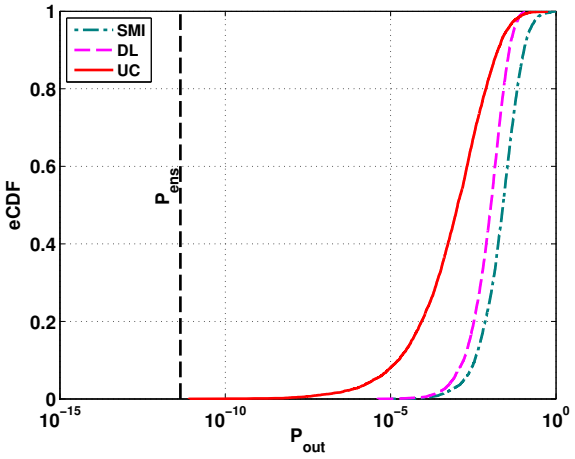

Fig. 4. Comparison of interferer output power empirical CDF between UC MVDR, SMI MVDR and DL MVDR beamformers with $N = 11$ element ULA and $L = 12$ snapshots.

former equal. Over the observed power output range, the UC MVDR beamformer has higher probability of achieving lower output power compared to both SMI MVDR and DL MVDR beamformers. The median output power of UC MVDR was more than 20 times lower than SMI MVDR and about 10 times lower than DL MVDR beamformer. Thus the UC MVDR suppresses the interferer better than both SMI MVDR and DL MVDR beamformers. Moreover, the UC MVDR has another advantage over the DL MVDR because it does not require an *a priori* choice of a tuning parameter like the DL factor.

Figure 5 compares the WNG for the UC MVDR against the SMI MVDR beamformer for same Monte Carlo experiment used to generate Figure 4. The optimal WNG for the experiment is 11. The histograms in Figure 5a show the improvement in WNG using the UC MVDR compared to SMI MVDR beamformer for same set of data. The dashed vertical denotes the ensemble WNG of 10.473. The UC MVDR beamformer has a higher probability of achieving higher WNG with an average WNG of 5.672 compared to an average WNG of 2.629 using the SMI MVDR beamformer. The scatter plot in 5b shows that the UC MVDR has a higher WNG than SMI MVDR beamformer in each trial instance except for small number of cases (bottom left corner in Figure 5b) where both beamformers have low WNG.

6. CONCLUSION

This paper presents the UC MVDR beamformer derived by moving the SMI MVDR zeros to lie on the unit circle. By placing zeros on the unit circle, the UC MVDR beampattern has perfect notches and lower sidelobes when compared to the SMI MVDR beampattern. Numerical simulations show that the UC MVDR beamformer suppresses interferers better than the SMI MVDR and DL MVDR beamformers and has higher average WNG than the SMI MVDR beamformer for the single interferer case.

7. REFERENCES

[1] H. L. Van Trees, *Detection, Estimation, and Modulation Theory, Optimum Array Processing*. John Wiley & Sons, 2002.

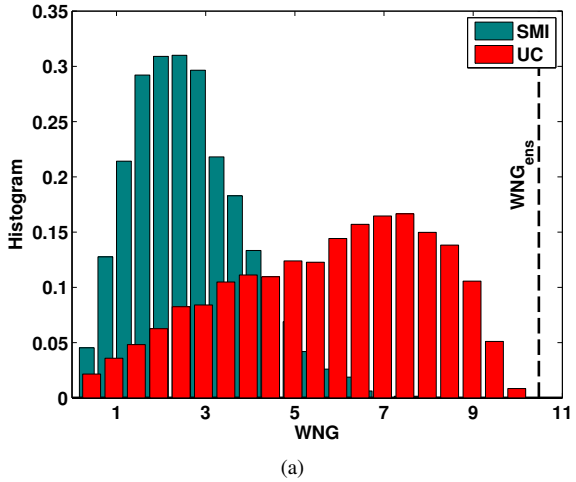

(a)

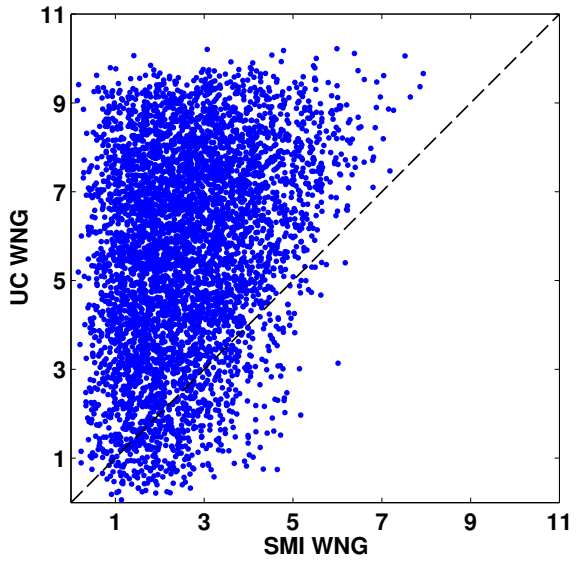

(b)

Fig. 5. Comparison between WNG for UC MVDR and SMI MVDR beamformer with $N = 11$ element ULA and $L = 12$ snapshots.

[2] J. Capon, "High-resolution frequency-wavenumber spectrum analysis," *Proc. IEEE*, vol. 57, no. 8, pp. 1408–1418, Aug. 1969.

[3] S. Schelkunoff, "Mathematical Theory of Linear Arrays," *Bell System Technical Journal*, vol. 22, no. 1, pp. 80–107, 1943.

[4] A. V. Oppenheim and R. W. Schafer with J. R. Buck, *Discrete-Time Signal Processing*, 2nd ed. Prentice-Hall Englewood Cliffs, 1999.

[5] B. D. Steinberg, *Principles of aperture and array system design: Including random and adaptive arrays*, 1st ed. John Wiley & Sons, 1976.

[6] A. Nehorai, "A minimal parameter adaptive notch filter with constrained poles and zeros," *IEEE Trans. Acoust., Speech, Signal Process.*, vol. 33, no. 4, pp. 983–996, Aug. 1985.

[7] B. Friedlander and J. O. Smith, "Analysis and performance

evaluation of an adaptive notch filter," *IEEE Trans. Inf. Theory*, vol. 30, no. 2, pp. 283–295, Mar. 1984.

[8] J. J. Shynk and B. Widrow, "Bandpass adaptive pole-zero filtering," in *International Conference on Acoustics, Speech, and Signal Processing*, vol. 11, Apr. 1986, pp. 2107–2110.

[9] J. Riba, J. Goldberg, and G. Vazquez, "Robust beamforming for interference rejection in mobile communications," *IEEE Trans. Signal Process.*, vol. 45, no. 1, pp. 271–275, 1997.

[10] A. B. Baggeroer and H. Cox, "Passive sonar limits upon nulling multiple moving ships with large aperture arrays," *Thirty-Third Asilomar Conference on Signals, Systems, and Computers*, vol. 103, no. 4, pp. 103–108, 1999.

[11] I. S. Reed, J. D. Mallett, and L. E. Brennan, "Rapid convergence rate in adaptive arrays," *IEEE Trans. Aerosp. Electron. Syst.*, vol. 10, no. 6, pp. 853–863, November 1974.

[12] B. Carlson, "Covariance matrix estimation errors and diagonal loading in adaptive arrays," *IEEE Trans. Aerosp. Electron. Syst.*, vol. 24, no. 4, pp. 397–401, Jul 1988.

[13] X. Mestre and M. A. Lagunas, "Diagonal loading for finite sample size beamforming: an asymptotic approach," in *Robust Adaptive Beamforming*. Wiley Interscience, John Wiley and Sons, 2005.

[14] E. N. Gilbert and S. P. Morgan, "Optimum design of directive antenna arrays subject to random variations," *Bell System Technical Journal*, vol. 34, no. 3, pp. 637–663, 1955.

[15] H. Cox, R. Zeskind, and M. Owen, "Robust adaptive beamforming," *IEEE Trans. Acoust., Speech, Signal Process.*, vol. 35, no. 10, pp. 1365–1376, Oct. 1987.

[16] A. Steinhardt and J. Guerci, "STAP for RADAR: what works, what doesn't, and what's in store," in *Proceedings of the IEEE Radar Conference*, April 2004, pp. 469–473.